journal

J. Am. Ceram. Soc., 94 [11] 4045–4051 (2011)
DOI: 10.1111/j.1551-2916.2011.04673.x

The Orientation Distributions of Lines, Surfaces, and Interfaces around Three-Phase Boundaries in Solid Oxide Fuel Cell Cathodes

Shen J. Dillon,[‡] Lam Helmick,[§,¶] Herbert M. Miller,[§] Lane Wilson,[¶,||] Randall Gemman,[¶] Rumyana V. Petrova,[§,††] Katayun Barmak,[§] Gregory S. Rohrer,[§] and Paul A. Salvador[§,¶,†]

[‡]Department of Materials Science and Engineering, University of Illinois, Urbana, Illinois, 61801

[§]Department of Materials Science and Engineering, Carnegie Mellon University, Pittsburgh, Pennsylvania, 15213

[¶]National Energy Technology Laboratory (NETL), Morgantown, West Virginia, 26507

Three-dimensional electron backscatter diffraction was used to measure the crystallographic distribution of the electrochemically relevant triple phase boundary lines and surfaces near them in SOFC cathodes made up of a porous mixture of yttria-stabilized zirconia and lanthanum strontium manganese oxide, both before and after mild electrochemical loading. All distributions were observed to be nearly isotropic, but non-random textures above the detection threshold were observed. The distributions differ between the two cells, as do the phase fractions and the electrochemical history. The different distributions are interpreted as evidence that steady-state distributions vary locally with phase fractions or that they evolve during the initial operation of the fuel cell. The rates at which triple lines, pore surfaces, and interface boundaries in the porous mixture approach a steady-state value appear to decrease with the average amount of mass transport required to reorient that specific feature. This work provides initial insights into the crystallography of interfaces in a multiphase ceramic material.

I. Introduction

The active cathode regions of many solid oxide fuel cells (SOFCs) considered for electrical power sources consist of three-phase mixtures of $La_{0.8}Sr_{0.2}MnO_3$ (LSM), Y_2O_3-stabilized ZrO_2 (YSZ), and pore space.[1–4] For oxygen reduction to occur, electrons from the LSM must reduce oxygen from the pore to form oxide ions within the YSZ.[5,6] The geometric feature that brings these three species together is known as the triple phase boundary (TPB): the line of the intersection between the YSZ, LSM, and vapor phases. Cathode performance relates to the distribution and activity of TPBs.[7–11] As oxygen reduction involves adsorption, surface diffusion, and bulk diffusion,[1,5,6] which are generally anisotropic, it is likely that oxygen reduction rates at TPBs also vary with crystallographic character.[12,13]

The complex features of electrodes, such as TPB length, have recently been correlated with their electrochemical activity.[5,9–11,14–18] Little is known about whether the microstructure of SOFCs has reached a steady-state distribution after processing or operation. SOFCs often exhibit an initial variation in performance, frequently an improvement called the burn-in effect,[19–21] as well as longer term degradation effects.[21] Portions of these performance variations may be related to small-scale microstructural changes.[21–23] While it is possible to estimate the TPB content from a stereological analysis of plane sections, such estimates are accurate only if the structure is isotropic.[7,24,25] To make direct measurements of the TPB content and their connectivity, Wilson *et al.*[9,10,14,15] made three-dimensional reconstructions of active anode regions from images of parallel serial sections collected using focused ion beam (FIB) milling in concert with scanning electron microscopy (SEM) imaging. They found that the TPB tortuosity was roughly isotropic in optimal electrodes. However, a fraction of the TPBs were not interconnected and could not contribute to the cell's electrochemical processes.[9,10,14,15] Using similar techniques, the microstructural characteristics in the cathode, including the porosity, TPB length, surface area, and tortuosity of each phase, were correlated with cell performance.[11,16–18,26,27]

There are two reasons why the crystallography of SOFC microstructures has not yet been explored. The first reason is application related: there is no clear path to establishing the importance of observed crystallographic features to SOFC performance, even though it is well known that surface properties are strongly coupled to crystallographic features, including oxygen surface exchange for YSZ[12] and LSM.[13] Modeling efforts that incorporate such data have been developed for other applications, such as modeling the mechanical response of microstructures.[28–30] The generation of appropriate data on surface properties and microstructures of cathodes will afford a complete model of activity that includes crystallography. The second reason is experimental: only recently have routine experimental and analytical techniques been developed to quantify these features,[31–35] and they have not been applied to any SOFC-related system.

There are very few quantitative investigations of the crystallography of microstructural features in two-phase complexes,[36,37] and none for three phase. Recently, we reported the quantitative characterization of the grain boundary population and energies for dense YSZ and demonstrated that small but statistically significant deviations from purely random distributions occur and are correlated with the experimentally observed energy anisotropies.[35] We have also carried out similar investigations on dense LSM, porous YSZ and LSM, and dense and porous YSZ/LSM mixtures, which provide information to analyze the SOFC microstructures with steady-state polycrystalline microstructures.[38] We observe that after typical SOFC sintering protocols, the microstructures reach steady-state distributions that are not

D. J. Green—contributing editor

Manuscript No. 29395. Received March 01, 2011; approved May 06, 2011.

This work was supported by the National Energy Technology Laboratory's on-going research in Materials Science & Engineering: SOFC under the RDS contract DE-AC26-04NT41817. This work was partially supported by the MRSEC program of the National Science Foundation under Award Number DMR-0520425 and by the Pennsylvania DCED.

[||]Present Address: Office of Basic Energy Sciences U.S. Department of Energy 1000 Independence Avenue SW Washington D.C. 20585-1290

[††]Present Address: International Iberian Nanotechnology Laboratory Braga Portugal

[†]Author to whom correspondence should be addressed. e-mail: paulsalvador@cmu.edu

strongly perturbed by annealing at low-temperatures.[35,38] No work has explored how electrochemical loading affects steady-state distributions.

The development of steady-state crystallographic anisotropy at solid–vapor interfaces has long been understood via the Wulff construction.[39] Investigations into the evolution of the crystallographic character of solid–solid interfaces in single-phase materials (grain boundaries) reveal a number of interesting general phenomena relating to energy anisotropy.[35,40,41] Other microstructural features with anisotropic energies, such as interphase boundaries and triple lines, should also exhibit comparable behavior in more complex systems. However, investigations of these features in multiphase materials are absent in the literature.

In this article, we describe the crystallography of relevant microstructural features at the active triple phase boundaries, such as the orientations of surfaces, interfaces, and TPBs, in the active region of porous LSM/YSZ cathodes. To do so, electron backscatter diffraction (EBSD) mapping was combined with FIB–SEM to image serial sections of the active cathodes of SOFCs.[42] The distributions of orientations of solid–solid and solid–vapor interfaces are measured, as well as the orientations of the triple lines, in an as-reduced (AR) state and after mild electrochemical loading (EL) simulating burn-in conditions. The distributions of interface planes in the three-phase region are compared with distributions in single-phase and two-phase regions of the SOFC. In all cases, there are mild anisotropies observed in the distributions of TPBs and interfaces.

II. Experimental Procedure

Two anode (Ni/YSZ) supported single cells were purchased from InDEC (H. C. Stark, Selb, Germany) and operated in buttoncell configurations with Au current collectors. The cells consisted of a 600 μm porous NiO-8YSZ (8% Y_2O_3–ZrO_2) anode, a 5–10 μm dense 8YSZ electrolyte, and a two-layer LSM cathode: an ≈ 15 μm thick porous LSM/8YSZ as the "active" layer contacting the electrolyte and an ≈ 15 μm thick porous LSM layer as a current collector. One cell (the AR or as-reduced cell) was heated to 800°C and kept at open circuit using air on the cathode while the anode was exposed first to 5% H_2 in N_2 for 2 h and then pure H_2 for 2 h. Another cell (the EL or electrochemically loaded cell) was treated in the same fashion and then galvanostatically operated at 0.7 V with hydrogen as a fuel gas at 800°C for 24 h, after which the current density was stable versus time (as observed for this cell and other cells treated similarly but for longer times).

The SOFCs were cut in cross section so that regions containing a dense layer of YSZ (electrolyte), a three-phase layer containing pores, YSZ, and LSM (active cathode), and a layer of porous LSM (current collector) could be imaged simultaneously. The sample was mounted on a 45° pre-tilt stub using conductive carbon tape, such that the layers of the fuel cell were parallel to the stub surface.[34] A thin platinum film was sputtered onto the specimen surface to prevent charging. The dual beam FIB–SEM (Nova 600; FEI company, Hillsboro, OR) has an ion gun that is situated at an angle 52° away from the electron gun, which is directly above the sample mount. To mill the sample, it is rotated around the electron beam axis and then tilted 7° towards the ion gun, so that its surface normal (on the 45° mount) is normal to the ion beam. The sample is then rotated 180° and tilted 25° towards the electron backscatter detector (Hakari, EDAX, Mahwah, NJ), which forms a 70° angle between the sample surface and the electron gun, which is ideal for EBSD mapping.

The samples were milled with a 30 kV, 500 pA Ga ion beam. The ion beam was used to remove 75 nm between each of 80 serial sections. EBSD data were obtained using a 20 kV, 9.5 nA electron beam. The data were collected on a hexagonal grid with 75 nm step size. EBSD patterns were collected relatively slowly (30 s^{-1}) to ensure that the two phases were well indexed and differentiated from each other. As it is important to distinguish pores, the analysis settings were optimized so that the solid phases were properly indexed and pores remained un-indexed. Over 5.3 and 6.6 million data points were recorded for the AR and EL samples, respectively. The data collection rate and desired point-to-point resolution ultimately limit the analyzed sample volume. The cells are indexed in cubic reference frames, with LSM in a cubic perovskite structure having a ≈ 3.88 Å[43,44] and with YSZ as a cubic fluorite structure with a = 5.15 Å.[45] The OIM software[46] was set so that if a minimum of four bands could not be identified in the EBSD patterns, the point is un-indexed and assumed to be part of the pore structure. All of the un-indexed points in the pores were assigned unique Euler angles ($\varphi_1 = 0$, $\Phi = 0$, $\varphi_2 = 0$) and a single grain ID so that groups of un-indexed points larger than a minimum grain size (10 pixels) would not be influenced by the clean-up procedure.[46] The clean-up procedure included assigning individual grains a single average orientation and using dilation to remove grains smaller than 10 pixels in area (<1% of the area of an average grain). By assigning indexed values to the pores, they did not preferentially shrink during dilation. The orientation values could then be subsequently removed from the pore pixels using the unique grain ID. The OIM software was used to extract line segments representing the grain boundary traces from each two-dimensional EBSD map.[46] The segments deviate by, at most, two pixels from the true boundary position.

To extract the three-dimensional crystallographic information, the planar sections were aligned as described in detail for a recent analysis of yttria.[34] Using these data, we determine three quantities. The first is the TPB distribution, which is the relative length of TPBs in a specific crystallographic direction. The directions may be indexed in the reference frame of either the LSM or the YSZ grain. The second is the distribution of pore surface orientations. Separate distributions are calculated for the YSZ and LSM grains. The third distribution is the solid–solid interphase boundary distribution. This is the distribution of interface orientations between LSM and YSZ and this distribution can be calculated in either the LSM or YSZ reference frames. These distributions were calculated only for features adjacent to TPBs. The features adjacent to the TPBs are the ones relevant to electrochemical activity[7–11]; by considering this single set of features, comparisons can be made between volumes with sufficient TPB populations, but with local variations in phase fractions and distributions.

The domain of possible orientations for the interfaces and triple lines was discretized according to the procedures described in reference [47]. The resolution is approximately 5° and this means that there are roughly 841 discrete orientations. The numbers of TPBs characterized in the as reduced (1500) and loaded (4000) cells were sufficient to populate these bins. The distributions are normalized to multiples of a random distribution unit, where a value of one corresponds to the number of observations expected in a random distribution. As the discretization and binning of the space can lead to small deviations from unity, sets of randomly generated TPBs were also considered. These ideally random distributions had peaks as high as 1.05 MRD and minima as low 0.95 MRD. Therefore, values of the distributions within these bounds will be interpreted as random. Surface dihedral angles at TPBs were calculated using the scalar product of the surface normal vectors. These data were binned with respect to the interface normal of the solid–solid boundaries in both the LSM and YSZ reference frames.

III. Results

A representative uncleaned EBSD map from a single serial section of the AR cell is shown in Fig. 1(a). The cells are

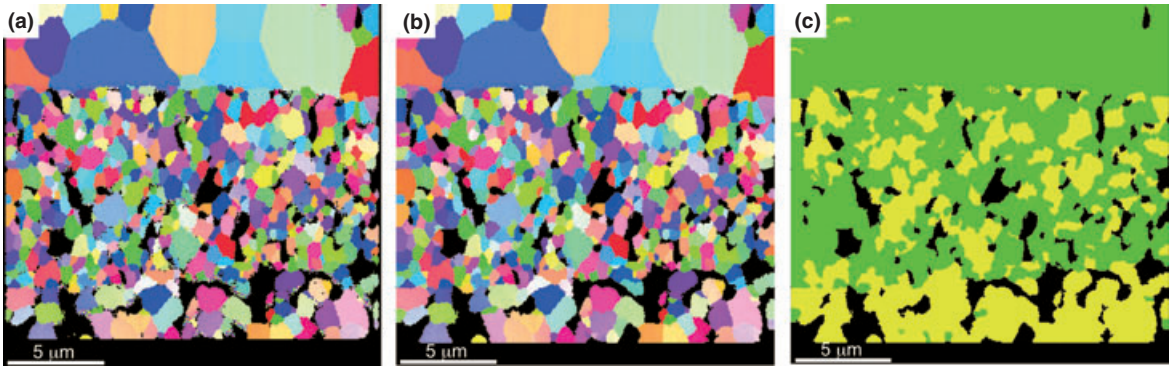

Fig. 1. Representative orientation, as inverse pole figures in (a) and (b), and phase (c) maps of the active cathode region in cross-section of the AR cell. The overall dimensions are 20.5 μm in the horizontal direction and 19.6 μm in the vertical direction. The raw orientation data are given in (a) and the cleaned data in (b). Colors represent different absolute orientations. In the phase map, green indicates YSZ, yellow indicates LSM, and black indicates pores.

indexed in cubic reference frames and the colors represent differently oriented grains. The large grains at the top of the image are from the dense YSZ electrolyte and the grains on the bottom are from the active cathode/porous LSM current collector interface. There are relatively few un-indexed pixels in the raw data outside of pores, indicating that the software indexes all solid regions well. A representative EBSD map from the cleaned data of the same serial section is shown in Fig. 1(b). Comparisons between Fig. 1(a) and (b) show that the clean up procedure does not distort the microstructural features. A phase map of the cleaned data is shown in Fig. 1(c). Green regions represent YSZ grains (the electrolyte is almost uniformly green), while yellow regions represent LSM grains (the current collector is almost uniformly yellow). Our observations indicated that the phase assignment is 90%–95% accurate. Oblique projections of the three-dimensional dataset for the AR cell are shown in Fig. 2; the sampled volume includes 80 slices. Similar results were obtained for the EL cell, where the volume of characterized region was 25.8 μm × 14.9 μm × 4.725 μm = 1816 μm^3.

The active cathode regions of the two cells were between 10 and 15 μm thick. The total volume of active cathode considered (after cropping the data) was 607 μm^3 in the AR cell and 1077 μm^3 in the EL cell. In the AR cell, the YSZ, LSM, and pore volumes were 63%, 28%, 9%, respectively. In the EL cell, the YSZ, LSM, and pore volumes were 71%, 11%, and 18%, respectively. The variation in the volumes of each phase was believed to be related to the small sampling volumes and the natural variation in the phase distributions in local regions of the cells,[16] which we observed here in larger 2-D areas as well. The numbers of TPBs characterized in the AR and EL cells were 1500 and 4000, respectively. These numbers were deemed sufficient to generate an accurate statistical description of the triple phase boundary distributions.

In Fig. 3, the TPB distributions of the active cathode regions are shown for the AR (a and b) and EL (b and c) cells. The TPBs show a preference for alignment along the <111> directions, whether they are indexed in the reference frame of YSZ (a and c) or LSM (b and d). The TPBs also have a significantly decreased preference for <001> directions.

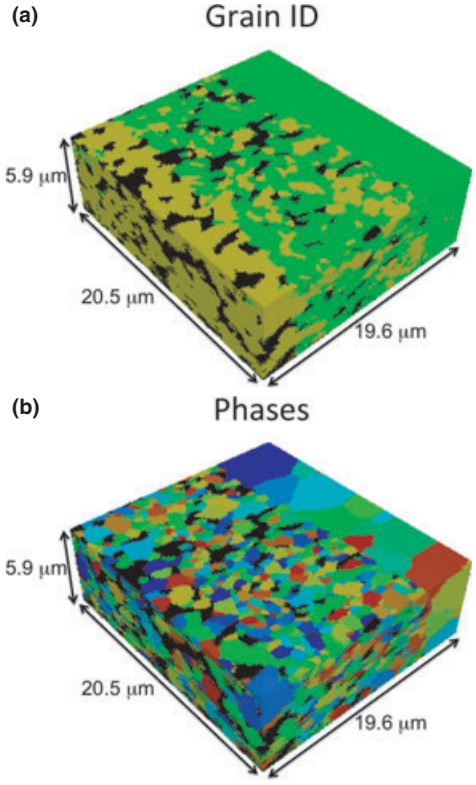

Fig. 2. Oblique projections of the reconstructed three-dimensional volume from the AR cell. The overall dimensions are 20.5 μm × 19.6 μm × 5.925 μm = 2381 μm^3. In the orientation map in (a), different colors are used to indicate different grains. In the phase map (b), green indicates YSZ, yellow indicates LSM, and black indicates pores.

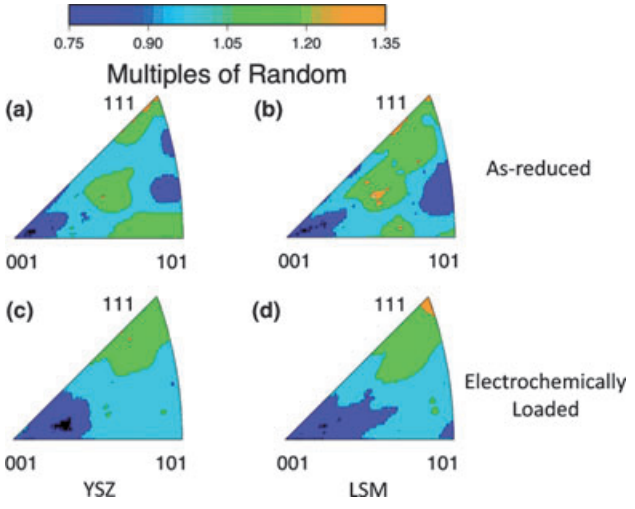

Fig. 3. Orientation distributions of the TPBs indexed in the YSZ reference frame (a and c) and in the LSM reference frame (b and d) in the AR cell (a and b) and the EL cell (c and d). Each distribution is given in a standard cubic stereographic triangle, where the colors indicate the multiples of random distribution with the legend given above (as is true in all figures herein).

Slight maxima are observed along the <110> and near the <531> directions in the AR states. These distributions are slightly affected by electrochemical loading. A small reduction in anisotropy of TPBs in the YSZ reference frame is observed after electrochemical loading. Generally, a more pronounced <111> preference and a reduction in the slight maxima at other locations are observed after electrochemical loading.

In Fig. 4, the distribution of YSZ (a and c) and LSM (b and d) surfaces adjacent to the TPBs are shown in the AR (a and b) and EL (c and d) samples. In the AR sample, the YSZ surfaces are distributed between {330} and {331}, and the {001} orientation is not favored. The distribution of YSZ surfaces is significantly altered by electrochemical loading. First, the distribution has less anisotropy than the surfaces in the AR sample. The YSZ surfaces adjacent to TPBs in the EL sample have a preference for {100} planes, in direct contrast to the AR cell. For the LSM surfaces, orientations near {100} and {110} are the most prevalent in the AR sample. The surface character of LSM next to the TPBs in the EL sample has a decreased anisotropy to that in the AR cell, but a similar distribution.

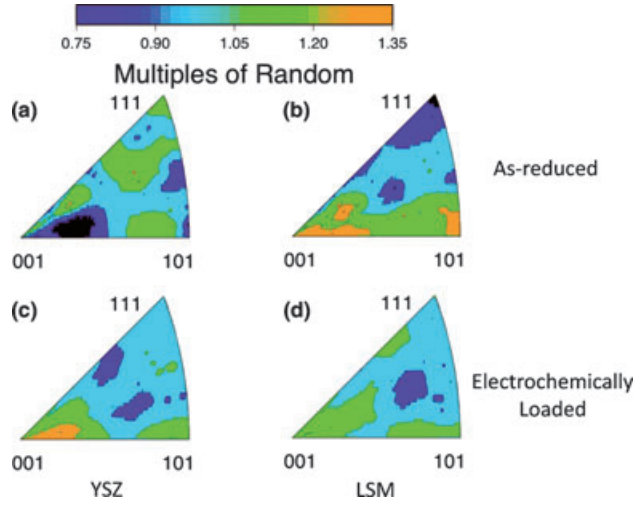

Fig. 4. Orientation distributions of the pore interfaces adjacent to TPBs indexed in the YSZ reference frame (a and c) and in the LSM reference frame (b and d) in the AR cell (a and b) and the EL cell (c and d).

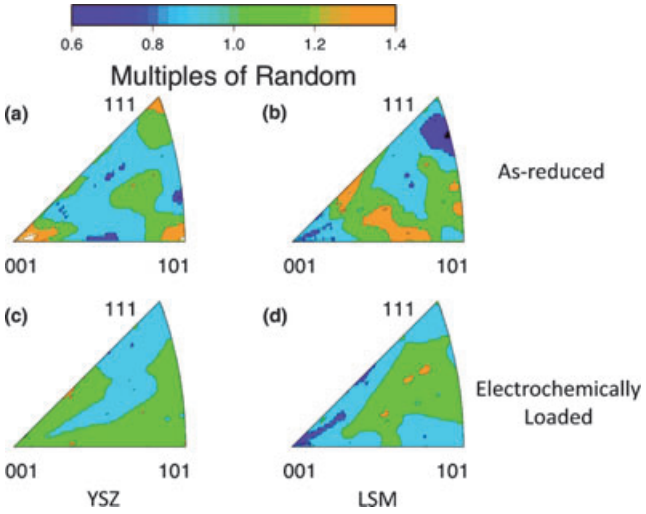

Fig. 5. Orientation distributions of the YSZ/LSM interfaces adjacent to TPBs indexed in the YSZ reference frame (a and c) and in the LSM reference frame (b and d) in the AR cell (a and b) and the EL cell (c and d).

The solid–solid interface plane distributions of the AR (a and b) and EL cells (c and d) are shown in Fig. 5. Note that the orientations of the same interfaces are indexed in both the YSZ (a and c) and LSM reference frames (b and d). The YSZ distribution shows maxima at the low-index orientations, with a maximum at {100}. The distribution for LSM shows a number of peaks at higher index orientations. Note that these interface plane orientations are constrained to lie in the zones of the TPBs. For example, the peaks at {100}, {110}, and {111} in YSZ are consistent with the {111} and {110} zones in the TPB distribution. The distributions for the EL cells are similar, but more isotropic.

The distribution of surface dihedral angles around the TPBs is shown in Fig. 6; these too exhibit anisotropy. The average dihedral angles in the AR (a and b) and EL (c and d) cells are 114° and 120°, respectively. Overall, the dihedral angles are more isotropic in the EL cell. While there are peaks in the distributions, these peaks do not correlate well with the observed relative populations of the solid–solid interfaces relative to which they were binned. The absence of a correlation between the peaks in this distribution and the preference for certain interface planes (presumed to be low energy) is not unexpected considering the fact that the dihedral angle is determined by the interface energy, which is influenced independently by the terminating planes in both phases.

IV. Discussion

Weak texture is observed in the crystallographic distributions of TPB directions and surface normals of interfaces adjacent to the TPBs in the LSM/YSZ active cathode of SOFCs. We interpret the small anisotropies in the populations as indications that the different interfacial and TPB energies are also anisotropic. We have used similar techniques to address the distributions in a variety of related model systems[35,38] and will use those observations to inform the discussion below. While TPBs do not exhibit any relative change between the two cells, the distributions of two-phase interfaces differ in the investigated regions of the two cells. The difference between the two cells can be interpreted in two fashions: either as a change in the relative interfacial energies with electrochemical loading or from local variations in the phase distributions between the two different volumes. Both interpretations will be considered in the discussion below. Despite

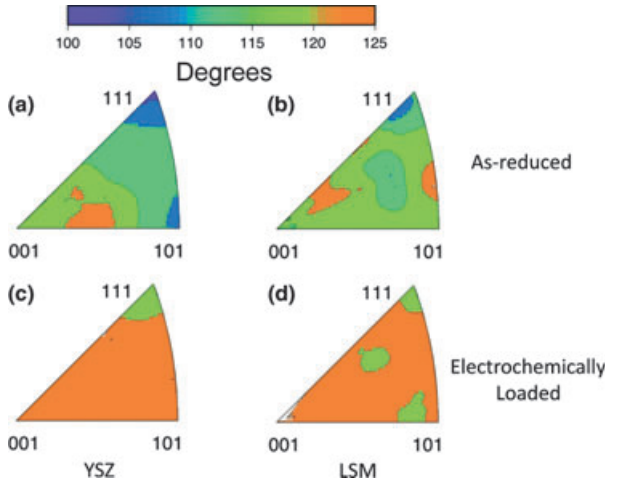

Fig. 6. Distribution of dihedral angles between pore surfaces adjacent to TPBs indexed in the YSZ reference frame (a and c) and in the LSM reference frame (b and d) in the AR cell (a and b) and the EL cell (c and d).

the difference in the phase distributions, the number of TPB boundaries observed was sufficient to generate a statistically appropriate representation of the misorientation averaged distributions of the microstructural features around the TPBs in both cells. These observations demonstrate that it is possible to accurately describe the electrochemically active components of SOFC cathodes.

The crystallographic preference in the distributions of TPBs weakly favors {111} and disfavors {100}, in both reference frames, and it does not vary significantly in either reference frame between samples. This is in spite of the fact that the distributions of the adjacent interfaces differ between the cells. These results suggest that the distributions of TPBs have a crystallographic preference and that they attain a stable state that is not affected by the volume fraction of phases/electrochemical history. The rate at which a particular distribution reaches some steady-state value may be interpreted with regard to thermodynamic and kinetic considerations. We assume that the TPB itself has negligible energy, of the same relative importance as that of a triple junction (TJ) line in a in single-phase polycrystal,[48] so that this distribution is not the driver for the overall microstructural evolution. We also assume that anisotropy exists in the TPB energy and this drives the local direction of the TPB line. To achieve the steady-state distribution, mass transport is required to reorient a TPB. At least two interfaces must change to reorient a TPB. As the amount of mass transfer required to reorient the TPB line is small in comparison with that required for other interfaces, the TPB is able to attain its steady-state distribution regardless of the other distributions.

The YSZ surface normals adjacent to TPBs weakly disfavor {100} in the AR cell but weakly favor {100} in the EL cell. The LSM surface normals adjacent to TPBs weakly favor {100} and {110} in the AR cell and have a similar but more isotropic preference in the EL cells. This indicates that the YSZ (LSM) surfaces adjacent to the triple phase boundaries are strongly (weakly) influenced by the local phase distributions and/or the electrochemical loading. Likewise, the LSM/YSZ interfacial distributions differ between the two cells, in both reference frames: the AR cell weakly favors the three low-index orientations in the YSZ reference frame and the high-index orientations in the LSM reference frame. The YSZ/LSM boundary normal distributions are qualitatively similar between the two cells, but the EL cell has a weaker anisotropy.

In dense single-phase materials, it has been observed that low-energy interfaces have larger relative areas than high-energy interfaces.[33,47,49] It has also been shown that the populations attain a steady-state distribution that is unaffected by further microstructural evolution. For reasons of the constraints discussed below, one should not expect the distributions of plane normals around the TPBs in three-phase composite materials to necessarily mimic the average distribution in dense or porous polycrystals of the component materials. A more complete description of the distributions of microstructural features around all TJs is required to correlate the TPB features to specific driving forces. The only available data on distributions of such features in cathode materials are from Helmick *et al.*[35] for dense YSZ and Helmick's recent Ph. D. Dissertation[38] for the remaining systems. For dense YSZ,[35] it was found that the grain boundary distributions closely matched the grain boundary energy distributions, even though they did not match the predicted distributions using surface energy or planar charge arguments. Also, steady-state values were obtained at typical SOFC sintering conditions and little thermal evolution occurred at SOFC operating conditions.[35] Similar results hold true in the other model systems,[38] including dense LSM, porous YSZ, porous LSM, dense LSM/YSZ, and porous LSM/YSZ, although the addition of another solid phase considerably reduces the grain size and consequently, the attainment of the steady-state condition. For the porous LSM/YSZ model system, the average grain sizes were under 1 μm, which are comparable to the length scales observed in the sintered cells described here. As such, we expect sintered cells to be close to a steady-state distribution from sintering; differences observed between the two cells here arise either from local variations in that state or from different electrochemical histories.

As the averaged distributions of interface normals from the 2-D work are similar to the interface normals around TPBs from this 3-D work, one can posit that similar energy landscapes control the microstructural evolution of these similar systems. In Helmick's work,[38] the weight fraction of the solids was 50 wt% YSZ with 50 wt% LSM; an amount of pore former was added that led to $\approx$ 25% porosity. In typical 2-D slices, the area fractions were $\approx$ 48% YSZ, 27% LSM, and 25% pores. This is to be compared with the volume fractions in the region of the AR cell tested here of 63%, 28%, 9%, respectively for YSZ, LSM, and pores. Helmick found that the addition of pores to dense materials did little to alter the overall solid–solid boundary distributions, but that the addition of other solid phases did alter the individual distributions. In particular, the LSM/LSM interfaces first attained steady state and seemed to dominate the microstructural evolution, strongly perturbing the YSZ interface distributions in two- and three-phase mixtures. The reasonable similarity in the LSM content between the interrogated region of the AR cell and those of Helmick's work may be the reason that similar distributions were obtained. In the interrogated region of the EL sample, the volume fractions were 71%, 11%, and 18%, respectively for YSZ, LSM, and pores. The local reduction in LSM content in this region may account for the difference in the distributions observed around the TPBs. If the TPB distributions are influenced by other TJ energy distributions, specifically those with LSM/LSM interfaces, and topological constraints, as proposed by Helmick,[38] then distributions similar to porous YSZ would be found in regions with low LSM contents. The {001} YSZ surface preference is in agreement with porous YSZ samples.

A second interpretation concerning the difference between the AR cell and the EL cell is that the crystallography of the electroactive microstructural features is influenced by the operational conditions. A variety of reports discuss the cathode conditioning effects and have related them to compositional and microstructural changes.[5,19–21,50–52] Research has focused on the fact that the surface Sr concentration is a function of the electrochemical conditioning. Although the effect of surface composition on surface energy is not known, Gorte and co-workers[53–55] have shown that the wetting characteristics of LSM on YSZ change with temperature and electrochemical load, and argued that the conditioning is related to these wetting characteristics, especially in infiltrated systems. Changes in wetting characteristics are directly related to relative changes in surface energies, which could manifest themselves as changes in the relative distributions. In this interpretation, one should consider if the thermodynamics and kinetics of redistribution of microstructural features are consistent with the observed distribution changes.

The dihedral angle data in Fig. 6 show that the ratio of the solid–solid interface energy to the surface energies in the EL cell is less than in the AR cell. The dihedral angle between pore surfaces is a nearly isotropic 120° and has a narrow spread in the EL cell, compared with the dihedral angle of 114° and the wider spread in the AR cell. That the dihedral angle distribution in the AR cell does not correlate well with the populations supports the idea that the energies of other features in the microstructure control the populations of surfaces at the TPBs in the AR cell. In the EL cell, the narrow distributions make it more difficult to assess the correlation between angles and populations, but it appears that in the more isotropic TPBs, a better correlation exists. These observations could be consistent with both interpretations of the origin of the observed populations. The change

in the TPB angle distributions indicates a relative change in the surface energies around the TPBs. This can arise if the interfacial energies of the TPBs are influenced by the local phase composition or the electrochemical loading of the cells.

Assuming that the triple line itself has a negligible energy,[48] relative to the interfacial energies, the distributions of interfaces surrounding the TJs are determined by a combination of energetic, crystallographic, topological, and kinetic constraints. The energetic constraints are represented by the Herring[56] condition, which must be satisfied to balance the interfacial energies at the TJ. However, because the crystals share a line of intersection, there is a crystallographic constraint that the three interfaces must be in the same crystallographic zone as the TJ, while still balancing the interfacial energy. Therefore, the rotation of one interface to a strongly preferred (low energy) orientation will influence the orientations of the other interfaces. It is posited that in three-phase materials, the relative range of the interfacial energies at TJs will vary much more strongly than in dense polycrystals. For the surfaces adjacent to the TPBs presented here, the three interfaces at the TJ are an YSZ surface, an LSM surface, and an LSM/YSZ interface. One of the difficulties in interpreting the current distributions is that the TPBs are only one of several TJs that exist in the microstructure: there are also LSM/LSM/LSM, YSZ/YSZ/YSZ, LSM/LSM/Pore, and YSZ/YSZ/pore TJs. Topologically, all of these TJs must connect and maintain the phase distributions in the sample, while satisfying the Herring condition for each TJ and maintaining the crystallographic constraints of the TJ lines. Clearly, more work is required to identify the factors that have a dominant influence on the microstructure.

For the EL cell, one explanation for the distributions is that the locally reduced concentration of LSM leads to a change in driving force and interfacial energies during sintering. Another explanation for the loaded cell is that the initial burn-in period of electrochemical loading alters the local populations. The number of so-called critical events (where features are removed from the system) will be low during electrochemical loading because the scale of the microstructure does not change. The number density of surface orientations can still vary if the pores change shape. The change in the dihedral angle indicates that the pore shapes are indeed different, although the correlation with sintering or electrochemical loading needs to be verified. As all of the distributions are close to isotropic, small changes in the relative distributions could be manifested by relatively small shape changes in the equilibrium pore shapes, or by deviations described above for initial sintering variations owing to phase distributions. As such, it is reasonable that the observed changes could be manifest at the operational conditions.

It should be pointed out that we did not correlate any of these distributions with the number of electrochemically active TPBs (based on microstructural connectivity). Wilson *et al.*[11,15,27] have already made strong correlations with the overall performance of SOFC cathodes and the number of electrochemically active TPBs (as well as the overall tortuosity of the transport paths). Their results imply that the local performance will vary with phase fractions, tortuosity, and connectivity, which would also impact the local electrochemical driving forces for microstructural evolution considered in this work. Clearly, much more research is required to understand how the local electrochemical properties vary within cathodes, especially because degradation events, such as Cr-poisoning, are known to be correlated with local properties, not average properties.[57,58]

The last point of interest here is to discuss the impact of these observations on SOFC activity. While we do observe weak texture in the cathodes, one could reasonably approximate the distributions as isotropic. As little is known about how the interfacial orientations affect the electrochemical activity of LSM and YSZ,[12,13] models that describe the microstructure as isotropic crystallographically seem reasonable. If there are significant differences in properties with crystallography, then the distribution of local electrochemical activity will be much wider than predicted by the isotropic models. As we do not observe strong texture, the average surface/interface in SOFCs should be considered as an average high-index surface, not a low-index energetically preferred surface. Most computational efforts and many experimental efforts focus on low-index, low-energy surfaces to simplify the problem. It is important to demonstrate that such investigations inform our understanding of average high-index surfaces that are ubiquitous in current SOFC cathodes.

V. Conclusions

Weak texture is observed in the crystallographic distributions of TPB directions and surface normals of interfaces adjacent to the TPBs in the LSM/YSZ active cathode of SOFCs. The crystallographic preference in the distributions of TPBs weakly favors the {111} and disfavors the {100}, in both reference frames, and it does not vary significantly in either of the crystal reference frames. We conclude that the TPB is able to obtain its steady-state distribution regardless of other populations. The crystallographic preference in the distributions of YSZ surface normals adjacent to TPBs weakly disfavors the {100} in the AR cell, but weakly favors the {100} in the EL cell. The crystallographic preference in the distributions of LSM surface normals adjacent to TPBs weakly favors the {100} and {110} in the AR cell, and this distribution is simply more isotropic in the EL cells. These observations are consistent with results from model ceramics samples of LSM and YSZ reported elsewhere. We conclude that either the difference in LSM phase fraction or the difference in electrochemical history could explain the different distributions observed between the two cells, but both are important for understanding SOFC activity and evolution. Finally, we conclude that crystallography of microstructural features in complex microstructures can be quantified accurately using three-dimensional EBSD analysis.

Acknowledgment

The authors thank Christopher Johnson (NETL) for preparing the AR and EL cells and Kirk Gerdes (NETL) for project management and useful discussions.

References

[1]N. Q. Minh and T. Takahashi, Science and Technology of Ceramic Fuel Cells. Elsevier Science, Amsterdam, 1995.
[2]S. C. Singhal, "Science and Technology of Solid-Oxide Fuel Cells," *MRS Bull.*, **25** [3] 16–21 (2000).
[3]B. C. H. Steele and A. Heinzel, "Materials for Fuel-Cell Technologies," *Nature*, **414**, 345–52 (2001).
[4]P. Singh and N. Q. Minh, "Solid Oxide Fuel Cells: Technology Status," *Int. J. Appl. Ceram. Technol.*, **1** [1] 5–15 (2004).
[5]J. Fleig, "Solid Oxide Fuel Cell Cathodes: Polarization Mechanisms and Modeling of the Electrochemical Performance," *Ann. Rev. Mat. Res.*, **33**, 3361–82 (2003).
[6]S. B. Adler, "Factors Governing Oxygen Reduction in Solid Oxide Fuel Cell Cathodes," *Chem. Rev.*, **104** [10] 4791–843 (2004).
[7]F. Zhao, Y. Jiang, G. Y. Lin, and A. V. Virkar, "The Effect of Electrode Microstructure on Cathodic Polarization"; pp. 501–10 in Solid Oxide Fuel Cells VII. Vol. 2001-16, *Electrochemical Society Proceedings*, (2001).
[8]V. A. C. Haanappel, J. Mertens, D. Rutenbeck, C. Tropartz, W. Herzhof, D. Sebold, and F. Tietz, "Optimisation of Processing and Microstructural Parameters of LSM to Improve the Electrochemical Performance of Anode-Supported SOFCs," *J. Power Sources*, **141**, 216–26 (2005).
[9]J. R. Wilson and S. A. Barnett, "Solid Oxide Fuel Cell Ni-YSZ Anodes: Effect of Composition on Microstructure and Performance," *Electrochem. Solid-State Lett.*, **11** [10] B181–5 (2008).
[10]J. R. Wilson, M. Gameiro, K. Mischaikow, W. Kalies, P. W. Voorhees, and S. A. Barnett, "Three-Dimensional Analysis of Solid Oxide Fuel Cell Ni-YSZ Anode Interconnectivity," *Microsc. Microanal.*, **15** [1] 71–7 (2009).
[11]J. R. Wilson, J. S. Cronin, A. T. Duong, S. Rukes, H.-Y. Chen, K. Thornton, D. R. Mumm, and S. Barnett, "Effect of Composition of ($La_{0.8}Sr_{0.2}MnO_3$-Y_2O_3-Stabilized ZrO_2) Cathodes: Correlating Three-Dimensional Microstructure and Polarization Resistance," *J. Power Sources*, **195** [7] 1829–40 (2010).

[12]K. Sasaki and J. Maier, "Chemical Surface Exchange of Oxygen on Y2O3-Stabilized ZrO2," *Solid State Ion.*, **161** [1–2] 145–54 (2003).
[13]L. Yan, K. R. Balasubramaniam, S. Wang, H. Du, and P. A. Salvador, "Effects of Crystallographic Orientation on the Oxygen Exchange Rate of $La_{0.7}Sr_{0.3}MnO_3$ Thin Films," *Solid State Ion.*, in press (2011).
[14]J. Wilson, W. Kobsiriphat, R. Mendoza, H. Chen, J. Hiller, D. Miller, K. Thornton, P. Voorhees, S. Adler, and S. Barnett, "Three-Dimensional Reconstruction of a Solid-Oxide Fuel-Cell Anode," *Nat. Mater.*, **5** [7] 541–4 (2006).
[15]J. R. Wilson, W. Kobsiriphat, R. Mendoza, H.-Y. Chen, T. Hines, J. M. Hiller, D. J. Miller, K. Thornton, P. W. Voorhees, S. B. Adler, D. Mumm, and S. A. Barnett, "Three Dimensional Reconstruction of Solid Oxide Fuel Cell Electrodes Using Focused ion Beam - Scanning Electron Microscopy," *ECS Trans.*, **7**, 1879–87 (2007).
[16]D. Gostovic, J. R. Smith, D. P. Kundinger, K. S. Jones, and E. D. Wachsman, "Three-Dimensional Reconstruction of Porous LSCF Cathodes," *Electrochem. Solid-State Lett.*, **10** [12] B214–B217 (2007).
[17]D. Gostovic, K. A. O'Hara, N. J. Vito, E. D. Wachsman, and K. S. Jones, "Multiple Length Scale Characterization of Doped Lanthanum Manganate Composite Cathodes," *ECS Trans.*, **16** [51] 83–93 (2009).
[18]J. R. Smith, A. Chen, D. Gostovic, D. Hickey, D. Kundinger, K. L. Duncan, R. T. DeHoff, K. S. Jones, and E. D. Wachsman, "Evaluation of the Relationship Between Cathode Microstructure and Electrochemical Behavior for SOFCs," *Solid State Ion.*, **180** [1] 90–8 (2009).
[19]M. J. Jorgensen, S. Primdahl, and M. Mogensen, "Characterisation of Composite SOFC Cathodes Using Electrochemical Impedance Spectroscopy," *Electrochim. Acta*, **44**, 4195–201 (1999).
[20]S. Jiang and J. Love, "Origin of the Initial Polarization Behavior of Sr-Doped $LaMnO_3$ for O_2 Reduction in Solid Oxide Fuel Cells," *Solid State Ion.*, **138** [3–4] 183–90 (2001).
[21]H. Yokokawa, H. Tu, B. Iwanschitz, and A. Mai, "Fundamental Mechanisms Limiting Solid Oxide Fuel Cell Durability," *J. Power Sources*, **182** [2] 400–12 (2008).
[22]S. P. Jiang and W. Wang, "Sintering and Grain Growth of (La,Sr)MnO_3 Electrodes of Solid Oxide Fuel Cells Under Polarization," *Solid State Ion.*, **176**, 1185–91 (2005).
[23]S. Jiang and J. Love, "Observation of Structural Change Induced by Cathodic Polarization on (La,Sr)MnO_3 Electrodes of Solid Oxide Fuel Cells," *Solid State Ion.*, **158** [1–2] 45–53 (2003).
[24]B. Kenney, M. Valdmanis, C. Baker, J. G. Pharoah, and K. Karan, "Computation of TPB Length, Surface Area and Pore Size From Numerical Reconstruction of Composite Solid Oxide Fuel Cell Electrodes," *J. Power Sources*, **189** [2] 1051–9 (2009).
[25]S. Zhang, M. Lynch, A. M. Gokhale, and M. Liu, "Unbiased Characterization of Three-Phase Microstructure of Porous Lanthanum Doped Strontium Manganite/Yttria-Stabilized Zirconia Composite Cathodes for Solid Oxide Fuel Cells Using Atomic Force Microscopy and Stereology," *J. Power Sources*, **192** [2] 367–71 (2009).
[26]A. Chen, J. Smith, R. T. DeHoff, E. D. Wachsman, G. R. Bourne, and K. S. Jones, "Effect of Cathode Microstructure on the Cathode Polarization in the Sintered Strontium-Doped Lanthanum Manganite/Yttria Stabilized Zirconia Solid Oxide Fuel Cells," *Microsc. Microanal.*, **14**, 1442 (2008).
[27]J. R. Wilson, A. T. Duong, M. Gameiro, H.-Y. Chen, K. Thornton, D. R. Mumm, and S. A. Barnett, "Quantitative Three-Dimensional Microstructure of a Solid Oxide Fuel Cell Cathode," *Electrochem. Commun.*, **11** [5] 1052–6 (2009).
[28]G. Spanos, D. J. Rowenhorst, A. C. Lewis, and A. B. Geltmacher, "Combining Serial Sectioning, EBSD Analysis, and Image-Based Finite Element Modeling," *MRS Bull.*, **33** [6] 597–602 (2008).
[29]Y. Bhandari, S. Sarkar, M. Groeber, M. D. Uchic, D. M. Dimiduk, and S. Ghosh, "3D Polycrystalline Microstructure Reconstruction From FIB Generated Serial Sections for FE Analysis," *Comp. Mater. Sci.*, **41** [2] 222–35 (2007).
[30]S. J. Kim, D. H. Kim, K. H. Oh, A. D. Rollett, R. A. Lebensohn, and H. N. Han, "An Elastoplastic Finite Element Modeling Coupled With Orientation Image Based Micromechanical Approach"; pp. 103–6 in NUMIFORM 2010. Vol. 1252, *AIP Conference Proceedings* Edited by F. Barlat, Y. H. Moon and M. G. Lee. (2010).
[31]M. D. Uchic, M. A. Groeber, D. M. Dimiduk, and J. P. Simmons, "3D Microstructural Characterization of Nickel Superalloys via Serial-Sectioning Using a Dual Beam FIB-SEM," *Scripta Mater.*, **55** [1] 23–8 (2006).
[32]D. J. Rowenhorst, A. Gupta, C. R. Feng, and G. Spanos, "3D Crystallographic and Morphological Analysis of Coarse Martensite: Combining EBSD and Serial Sectioning," *Scripta Mater.*, **55** [1] 11–6 (2006).
[33]D. M. Saylor, A. Morawiec, and G. S. Rohrer, "The Relative Free Energies of Grain Boundaries in Magnesia as a Function of Five Macroscopic Parameters," *Acta Mater.*, **51** [13] 3675–86 (2003).
[34]S. J. Dillon and G. S. Rohrer, "Characterization of the Grain-Boundary Character and Energy Distributions of Yttria Using Automated Serial Sectioning and EBSD in the FIB," *J. Amer. Ceram. Soc.*, **92** [7] 1580–5 (2009).
[35]L. Helmick, S. J. Dillon, K. Gerdes, R. Gemmen, G. Rohrer, S. Seetharaman, and P. A. Salvador, "Crystallographic Characteristics of Grain Boundaries in Dense Yttria-Stabilized Zirconia," *Int. J. Appl. Ceram. Technol.*, in press (2011). DOI: 10.1111/j.1744-7402.2010.02567.x.
[36]C.-S. Kim, T. R. Massa, and G. S. Rohrer, "Modeling the Influence of Orientation Texture on the Strength of WC-Co Composites," *J. Am. Ceram. Soc.*, **90** [1] 199–204 (2007).
[37]C.-S. Kim and G. S. Rohrer, "Geometric and Crystallographic Characterization of WC Surfaces and Grain Boundaries in WC-Co Composites," *Interface Sci.*, **12**, 19–27 (2004).
[38]L. Helmick, "Microstructural Characterization of Solid Oxide Fuel Cell Cathode Materials"; Ph.D. Thesis in Materials Science and Engineering, Carnegie Mellon University, Pittsburgh, 2010.
[39]G. Wulff, "On the Question of the Rate of Growth and Dissolution of Crystal Surfaces," *Z. Kristallogr. Miner.*, **34**, 449–530 (1901).
[40]J. Gruber, H. M. Miller, T. D. Hoffmann, G. S. Rohrer, and A. D. Rollett, "Misorientation Texture Development During Grain Growth. Part I: Simulation and Experiment," *Acta Mater.*, **57** [20] 6102–12 (2009).
[41]S. J. Dillon and G. S. Rohrer, "Mechanism for the Development of Anisotropic Grain Boundary Character Distributions During Normal Grain Growth," *Acta Mater.*, **57** [1] 1–7 (2008).
[42]J. R. Izzo Jr., A. S. Joshi, K. N. Grew, W. K. S. Chiu, A. Tkachuk, S. H. Wang, and W. Yun, "Nondestructive Reconstruction and Analysis of SOFC Anodes Using x-ray Computed Tomography at sub-50 nm Resolution," *J. Electrochem. Soc.*, **155** [5] B504–8 (2008).
[43]E. O. Wollan and W. C. Koehler, "Neutron Diffraction Study of the Magnetic Properties of the Series of Perovskite-Type Compounds $La_{1-X}Ca_xMnO_3$," *Phys. Rev.*, **100**[2] 545 (1955).
[44]A. Hammouche, E. Siebert, and A. Hammou, "Crystallographic, Thermal and Electrochemical Properties of the System $La_{1-X}Sr_xMnO_3$ for High Temperature Solid Electrolyte Fuel Cells," *Mater. Res. Bull.*, **24** [3] 367–80 (1989).
[45]C. J. Howard and R. J. Hill, "The Polymorphs of Zirconia: Phase Abundance and Crystal Structure by Rietveld Analysis of Neutron and X-ray Diffraction Data," *J. Mater. Sci.*, **26** [1] 127–34 (1991).
[46]TSL Inc. "Orientation Imaging Microscopy Software Version 4.3 User Manual," EDAX, Mahwah, NJ. (2006).
[47]G. S. Rohrer, D. M. Saylor, B. El Dasher, B. L. Adams, A. D. Rollett, and P. Wynblatt, "The Distribution of Internal Interfaces in Polycrystals," *Z. Metallkd*, **95** [4] 197–214 (2004).
[48]B. Zhao, J. C. Verhasselt, L. S. Shvindlerman, and G. Gottstein, "Measurement of Grain Boundary Triple Line Energy in Copper," *Acta Mater.*, **58** [17] 5646–53 (2010).
[49]D. M. Saylor, A. Morawiec, and G. S. Rohrer, "Distribution and Energies of Grain Boundaries in Magnesia as a Function of Five Degrees of Freedom," *J. Amer. Ceram. Soc.*, **85** [12] 3081–3 (2002).
[50]S. B. Frank, F. Jurgen, K. Mitsuharu, S. Ulrich, H. Hanns-Ulrich, and M. Joachim, "Strong Performance Improvement of $La_{0.6}Sr_{0.4}Co_{0.8}Fe_{0.2}O_{3-\delta}$ SOFC Cathodes by Electrochemical Activation," *J. Electrochem. Soc.*, **152** [10] A2074–9 (2005).
[51]F. S. Baumann, J. Maier, and J. Fleig, "The Polarization Resistance of Mixed Conducting SOFC Cathodes: A Comparative Study Using Thin Film Model Electrodes," *Solid State Ion.*, **179** [21–26] 1198–204 (2008).
[52]K.-C. Chang, B. Ingram, K. R. Balasubramaniam, B. Yildiz, D. Hennessy, P. A. Salvador, N. Leyarovska, and H. You, "In Situ Synchrotron X-ray Studies of Dense Thin-Film Strontium-Doped Lanthanum Manganite Solid Oxide Fuel Cell Cathodes," *Mat. Res. Soc. Symp. Proc.*, **1126**, 1126–S08 (2009).
[53]Y. Huang, J. M. Vohs, and R. J. Gorte, "Characterization of LSM-YSZ Composites Prepared by Impregnation Methods," *J. Electrochem. Soc.*, **152** [7] A1347–53 (2005).
[54]Y. Huang, J. M. Vohs, and R. J. Gorte, "SOFC Cathodes Prepared by Infiltration With Various LSM Precursors," *Electrochem. Solid-State Lett.*, **9** [5] A237–40 (2006).
[55]J. M. Vohs and R. J. Gorte, "High-Performance SOFC Cathodes Prepared by Infiltration," *Adv. Mater.*, **21**, 943 (2009).
[56]C. Herring, "Theorems on the Free Energies of Crystal Surfaces," *Phys. Rev.*, **82**, 87–93 (1951).
[57]S. Wang, T. A. Cruse, M. Krumpelt, B. J. Ingram, and P. A. Salvador, "Microstructural Degradation of (La,Sr)MnO_3/YSZ Cathodes in Solid Oxide Fuel Cells With Uncoated E-Brite Interconnects," *J. Electrochem. Soc.*, **158** [2] B152–8 (2011).
[58]M. Krumpelt, T. A. Cruse, B. J. Ingram, J. L. Routbort, S. Wang, P. A. Salvador, and G. Chen, "The Effect of Chromium Oxy-Hydroxide on Solid Oxide Fuel Cells," *J. Electrochem. Soc.*, **157** [2] B228–33 (2010). □